AFRL-AFOSR-VA-TR-2015-0231

Plant-mimetic heat pipes for operation with large inertial and gravitational stresses

Abraham Stroock
CORNELL UNIVERSITY

07/08/2015
Final Report

Air Force Research Laboratory
AF Office Of Scientific Research (AFOSR)/ RTD
Arlington, Virginia 22203
Air Force Materiel Command

REPORT DOCUMENTATION PAGE

Form Approved
OMB No. 0704-0188

1. REPORT DATE *(DD-MM-YYYY)*	2. REPORT TYPE	3. DATES COVERED *(From - To)*
13-08-2015	Final Performance	01-05-2012 to 30-04-2015

4. TITLE AND SUBTITLE
Plant-mimetic heat pipes for operation with large inertial and gravitational stresses

5a. CONTRACT NUMBER

5b. GRANT NUMBER
FA9550-12-1-0227

5c. PROGRAM ELEMENT NUMBER
61102F

6. AUTHOR(S)
Abraham Stroock

5d. PROJECT NUMBER

5e. TASK NUMBER

5f. WORK UNIT NUMBER

7. PERFORMING ORGANIZATION NAME(S) AND ADDRESS(ES)
CORNELL UNIVERSITY
373 PINE TREE RD
ITHACA, NY 14850-2820 US

8. PERFORMING ORGANIZATION REPORT NUMBER

9. SPONSORING/MONITORING AGENCY NAME(S) AND ADDRESS(ES)
AF Office of Scientific Research
875 N. Randolph St. Room 3112
Arlington, VA 22203

10. SPONSOR/MONITOR'S ACRONYM(S)
AFRL/AFOSR RTD

11. SPONSOR/MONITOR'S REPORT NUMBER(S)

12. DISTRIBUTION/AVAILABILITY STATEMENT
A DISTRIBUTION UNLIMITED: PB Public Release

13. SUPPLEMENTARY NOTES

14. ABSTRACT
The design of heat transfer systems for applications in aircraft and other dynamic contexts involves stringent constraints on weight, form factor, breadth of operating conditions, and robustness of operation. Heat pipes have long been recognized as an attractive, passive alternative to conventional heat exchangers for these applications. Yet, the capillary limitation in conventional heat pipes limits their operation to contexts in which there exist minimal hydraulic, gravitation, and inertial stresses. In this project, we have exploited insights from the physiology of plants to propose plant-inspired designs of loop heat pipes for operation with large stresses. Toward the realization of these Superheated Loop Heat Pipes (SHLHP), we developed a set of mathematical models and experimental approaches. Our models provide design rules for heat transfer systems that could provide significant advantages relative to conventional designs. Our experimental platforms have led to unprecedented measurements on liquids at large negative pressures, insights into the dynamics of metastable liquids, and the prototypes of the first technologies to exploit liquids under tension

15. SUBJECT TERMS
Self-Cooling, Plant-mimetic, Heat Pipes

16. SECURITY CLASSIFICATION OF:			17. LIMITATION OF ABSTRACT	18. NUMBER OF	19a. NAME OF RESPONSIBLE PERSON
a. REPORT	b. ABSTRACT	c. THIS PAGE			Abraham Stroock

Unclassified	Unclassified	Unclassified	UU	**PAGES**	**19b. TELEPHONE NUMBER** *(Include area code)* 607-255-4276

Title: PLANT-MIMETIC HEAT PIPES FOR OPERATION WITH LARGE INERTIAL AND GRAVITATIONAL STRESSES

P.I.: Abraham Stroock, Chemical and Biomolecular Engineering, Cornell University
Co-P.I.: N. Michelle Holbrook, Organismic and Evolutionary Biology, Harvard University

Contract #: FA9550-12-1-0227

PM: Byung Lip Lee

I. Summary:

Heat pipes and loop heat pipes have long been recognized as attractive alternatives to conventional heat exchangers, but the limit in the magnitude of the capillary pressures generated by the wicks in conventional designs has placed a severe limit on their applicability in vehicles and other large-scale applications. In this project, we aim to overcome this limitation by designing heat pipes with nano-porous wicks that support 10s of bars of capillary pressure. To this end, we are developing design concepts for heat pipes operating in this new regime, developing new fabrication strategies for hierarchically structured wicks that maximize capillary pressures while maintaining reasonable hydraulic resistances, and elucidating the strategies exploited by vascular plants to manage large capillary pressures and the associate metastability of the liquid phase.

II. Objectives:

1. Develop of design concepts and tools for heat pipes operated with large capillary pressures.
2. Develop materials and fabrication methods to couple efficient, microfluidic paths with nanoporous membranes for the generation of large negative pressures.
3. Elucidate plant physiological mechanisms of operation and repair for the manipulation of liquids at large negative pressures.
4. Develop prototypes of negative pressure loop heat pipes with operation under subsaturated conditions.

III. Summary of progress:

In this funding period, we have made progress on a number of fronts:

1) Design concepts and modeling tools: We have proposed a new design for loop heat pipes that operates with superheated liquid and completed a mathematical model of steady state operation of such superheated loop heat pipes (SHLHP). We have also developed a transport theories for complex composites inspired by both xylem and leaf structures.

2) Materials and methods of fabrication: We have developed two strategies for coupling microfluidic structures to nanoporous membranes in order to capture critical features of the physiology of xylem for the movement of liquid under tension.

3) Dynamics of transport and phase change in plant mimetic micro-nanofluidic systems: We have elucidated the complex dynamics of cavitation processes in xylem-mimics and probed nano-confined capillary and flow with unprecedented resolution.

4) Integration and prototype development: We have integrated MEMS pressure sensing with xylem-mimetic microfluidics to allow for unprecedented mechanical measurements of negative

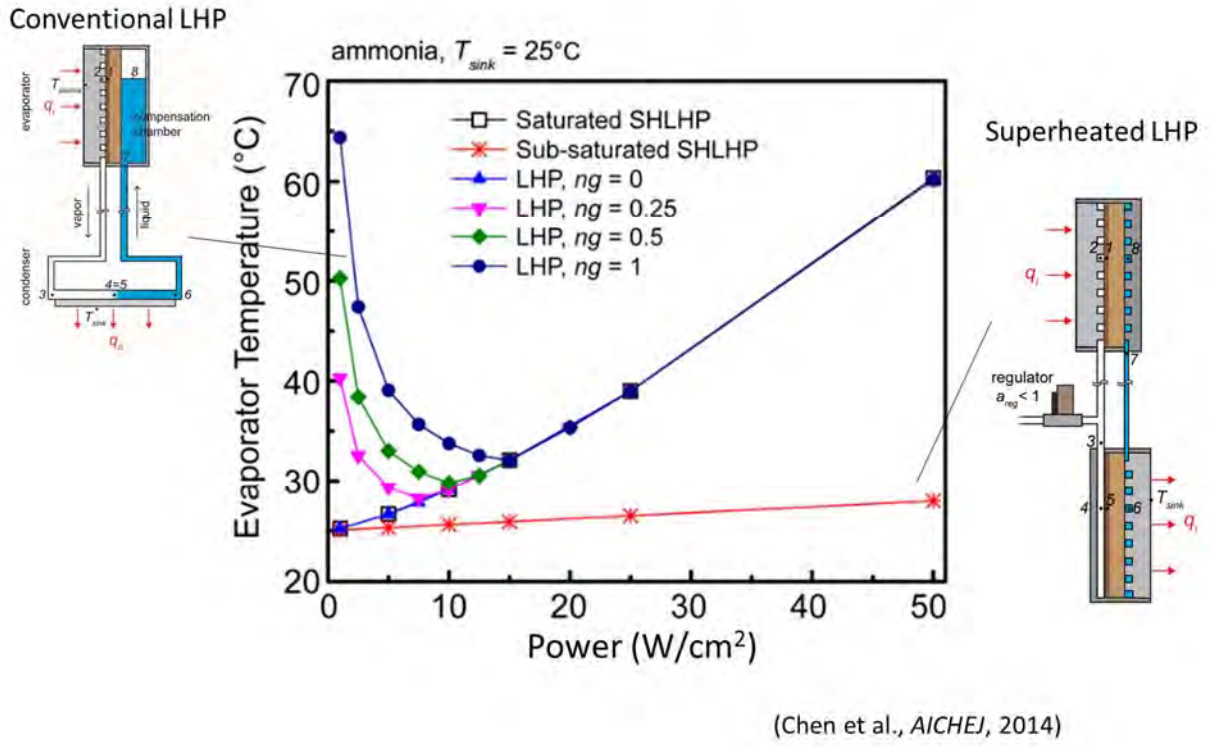

Figure 1: Model of superheated loop heat pipe (SHLHP). Predictions of evaporator temperature as a function of power density and adverse acceleration for conventional loop heat pipe (closed symbols), saturated superheated loop heat pipe (open squares) and sub-saturated superheated loop heat pipe (red asterisk). Parameters: ammonia as working fluid; total length from evaporator to condenser, L_{pipe} = 10 m; sink temperature, T_{sink} = 25 °C; adverse acceleration in number of gravity equivalents, ng = 0, 0.25, 0.5, and 1. Schematic diagrams of conventional LHP (top left) and sub-saturated SHLHP (right) are shown.

pressure and sensing of water status in the environment. We have also built complete liquid paths for the SHLHP and developed an experimental platform to characterize its function.

5) Physiology and biophysics of heat transfer and flow control in plant tissues. We have developed a successful theory of coupled heat and mass transfer within the composite, internal structure of leaves; this theory provides a basis for the design of generalized phase-change heat transfer materials. We have also elucidated a mechanism by which plants control the conductance of their leaves based on reversible collapse of the tissues surrounding their vessels.

IV. Detailed report:

Objective 1: Fundamental understanding of and design concepts for heat pipes for operation at negative pressures.

As we have reported previously, the a loop heat pipe capable of maintaining the liquid path at negative pressures offers two important benefits relative to conventional designs: 1) the ability to operate against large adverse accelerations without dry out and 2) the elimination of a major contributor to the thermal resistance in the form of condensate in the vapor path. We have proposed a new design for superheated loop heat pipes (SHLHP) that would allow for the exploitation of these features[1]. We reported a complete analysis of this design last year[2].

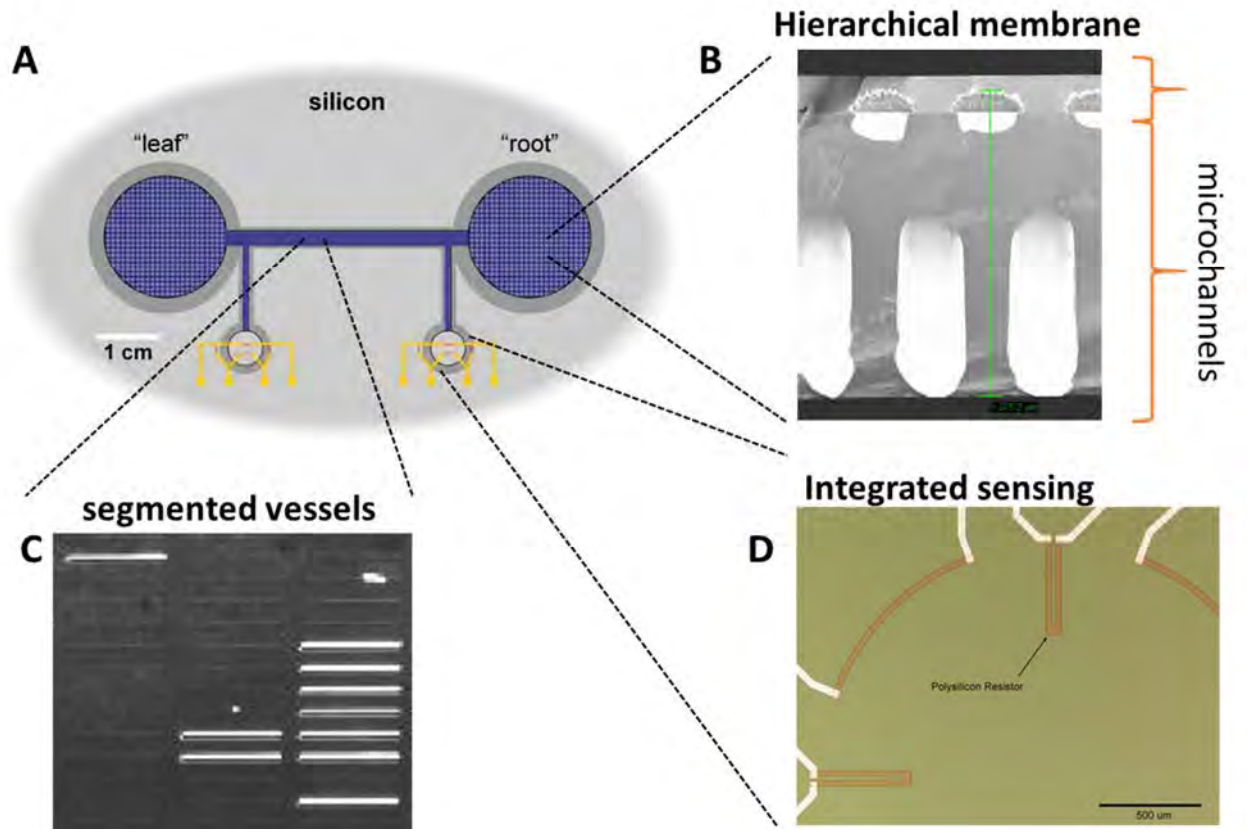

Figure 2: Silicon platform for plant-inspired SHLHP. (A) Schematic diagram of wick structure with integrated pressure sensors. **(B)** Hierarchical silicon membrane. **(C)** Micrograph of segmented vessels separated by nanoporous silicon. **(D)** Micrograph of a section of two branches of a Wheatstone bridge of poly(silicon) resistors on a silicon diaphragm.

Importantly, this analysis provides a new set of approximate solutions for the steady state operation of loop heat pipes (both conventional and superheated) that form the basis for simple design rules.

Figure 1 provides a synopsis of the predictions of our model for the evaporator temperature (~ source temperature) as a function of the applied thermal load. We compare three designs: 1) conventional LHP (filled symbols), 2) SHLHP operated in a saturated regime in which liquid is present in the vapor path (open squares – left-hand diagram), and 3) SHLHP operated in a sub-saturated regime in which no liquid is present in the vapor path (red asterisks – right hand diagram). We first note that the conventional design requires a large increase in evaporator temperature at low heat flux, as occurs at start-up. Furthermore, this spike in temperature grows rapidly with adverse acceleration (varied from 0 to 1 g). This requirement of elevated temperature is required in the conventional design because it is the vapor pressure that drives flow around the loop. This requirement is known to lead to instabilities upon start up and to dramatically limit operation of conventional LHPs in the presence of adverse acceleration.

With the elimination of vapor from the liquid path (filling the vapor space with liquid at point 8 in the left-hand diagram), one creates a saturated SHLHP. This change eliminates the require spike in temperature at low heat flux (open square) and the system become nearly completely insensitive to adverse acceleration. These changes occur because the fluid is now

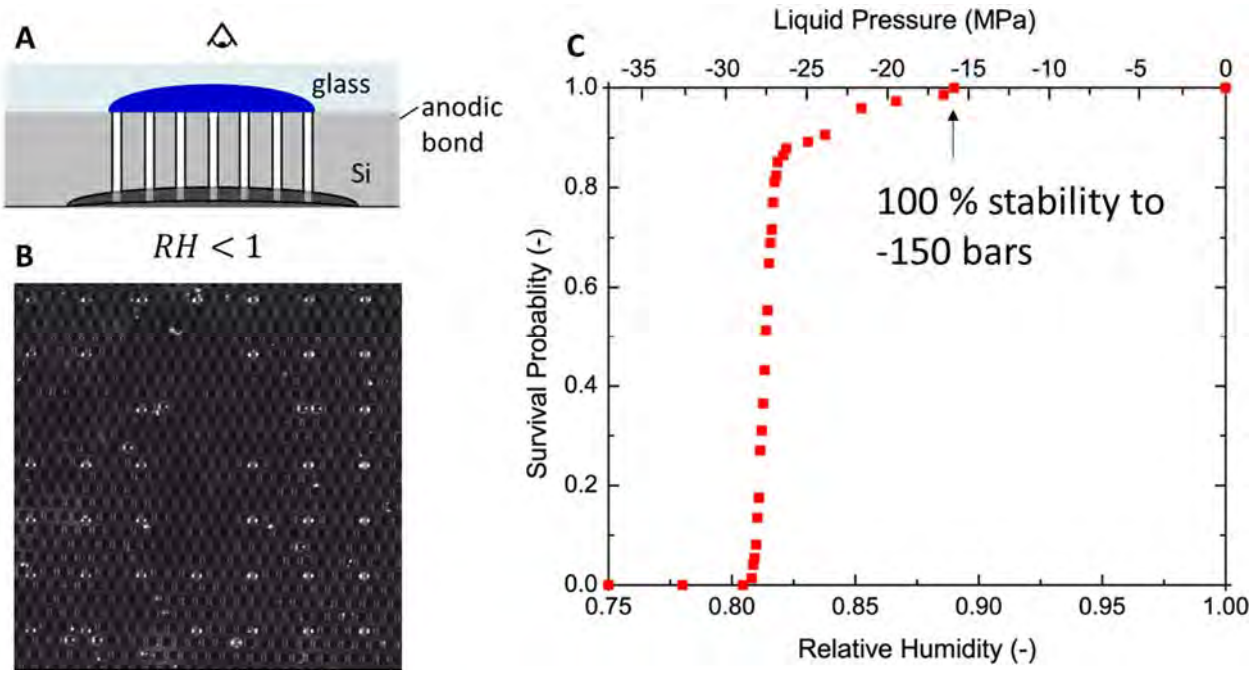

Figure 3: Stability limit of hierarchically structured silicon membrane. (**A**) Schematic cross-section of hierarchical membrane with reactive ion etched microchannels coupled to a thin layer of anodically etched, nano-porous silicon. A liquid-filled microfluidic cavitiy in glass is sealed to the top surface. (**B**) Micrograph showing top-view of system in (A). Empty cavities are visible. (**C**) Fraction of cavities (of 625) that remain filled with liquid as a function of relative humidity.

pumped around the loop by the reduction of pressure in the liquid rather than the increase in pressure in the vapor. On the other hand, in the saturated mode of operation, the SHLHP shows the same increase in evaporator temperature with increasing heat flux as the conventional design. In both cases, this increase results from the resistance to heat transfer of a condensate layer on the vapor-side of the condenser. The diagram on the right shows our design for a sub-saturated SHLHP in which we add two features: 1) a nanoporous membrane at the condenser; this addition allows the entire liquid path to operate at negative pressures. 2) A regulator valve in the vapor path to maintain a state of sub-saturation as temperature changes such that no liquid condenses in the vapor path. ***With these two modifications, the sub-saturated SHLHP shows significantly weaker dependence of the evaporator temperature on heat flux (higher effective thermal conductivity) because of the elimination of the condensate layer on the condensing surface. Furthermore, this response is independent of adverse acceleration so long as the liquid path remains intact.*** We predict that robust operation over large distances (10s of meters) requires the ability to manipulate liquids at -1-5 MPa within microchannels in the liquid path.

Objective 2: Develop materials and fabrication methods to couple efficient, microfluidic paths with nanoporous membranes for the generation of large negative pressures..

Figure 2 presents an overview of our approach for the formation of a wick structure for SHLHPs. The key elements of our design are: 1) appropriate membranes at the evaporator and condenser that can transfer large capillary stress to bulk liquid water in the liquid path (Figure 2B); 2) local structure along the liquid path that allows for cavitation events that do occur to be

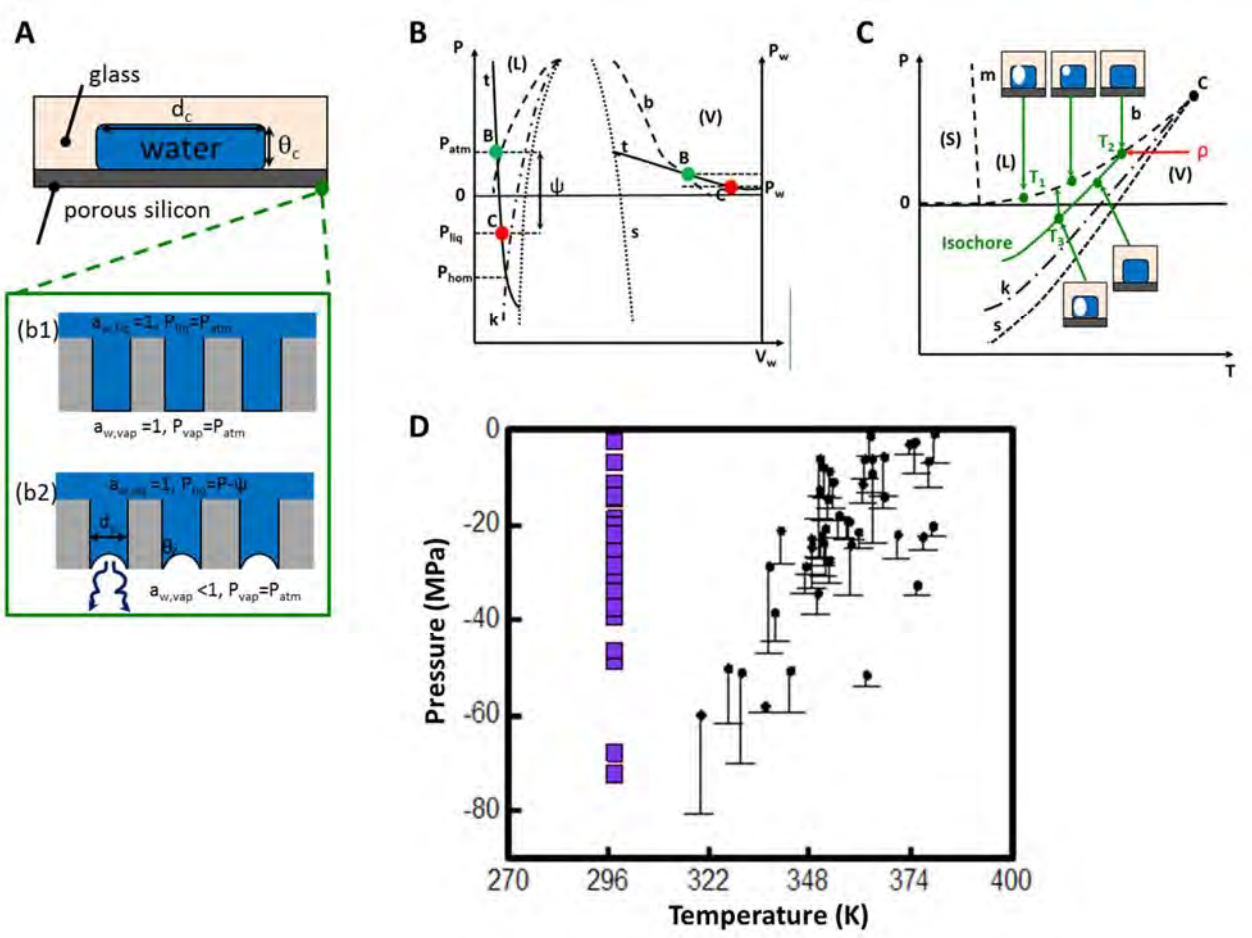

Figure 4: Extreme stability of liquid water under tension. **(A)** Schematic cross-sectional view of a liquid-filled cavity coupled via a nano-porous silicon membrane to an external vapor. (**B**) Schematic representation of metastable vapor-liquid equilibrium (MVLE) on an isotherm in the PV diagram of water. (**C**) Schematic representation of an isochoric path into tension in the PT diagram of water. (**D**) Pressures at cavitation observed along isothermal paths by MVLE (purple squares) and by isochoric cooling (black diamonds).

isolated and refilled (Figure 2C); and 3) pressure sensors to allow for monitoring the operational status of the pipe and the triggering of response to failure (Figure 2D).

Nano-porous membranes. The membranes at the evaporator and condenser of a heat pipe must host the liquid phase in small pores to generate capillary pressure differences with respect to the vapor phase, high thermal conductivity to minimized temperature gradients and unnecessary superheat, high hydraulic conductivity to avoid unnecessary pressure gradients and further superheat, and high elastic modulus to avoid deformation due to capillary stresses. Current heat pipe technologies use membranes (typically wire meshes) at the evaporator and condenser that present the liquid phase in pores of diameter > 1 μm; these membranes have high thermal conductivity and hydraulic permeability but generate less than 1 bar of capillary pressure.[3] We previously demonstrated an organic membrane capable of large stresses (> 20 MPa or 200 bars of tension), but this material presented poor thermal conductivity, permeability, and mechanics.[4] Under this program, we have developed the first examples of inorganic

membranes capable of sustaining substantial tensions. Our strategy is based on the use of anodic etching to form nano-scale pores in single crystalline silicon. This material provide appropriate mechanical strength, high thermal conductivity and compatibility with diverse microfabrication techniques to allow for tailored architectures.

We have explored the use of porous silicon in several formats and demonstrated that it is capable of maintaining capillary tensions to beyond -20 MPa[5,6]; we will discuss these published examples in the following sections. First, we report on two development from the last year of this funding period. **Figure 3** presents the characterization a hierarchically structured membrane of

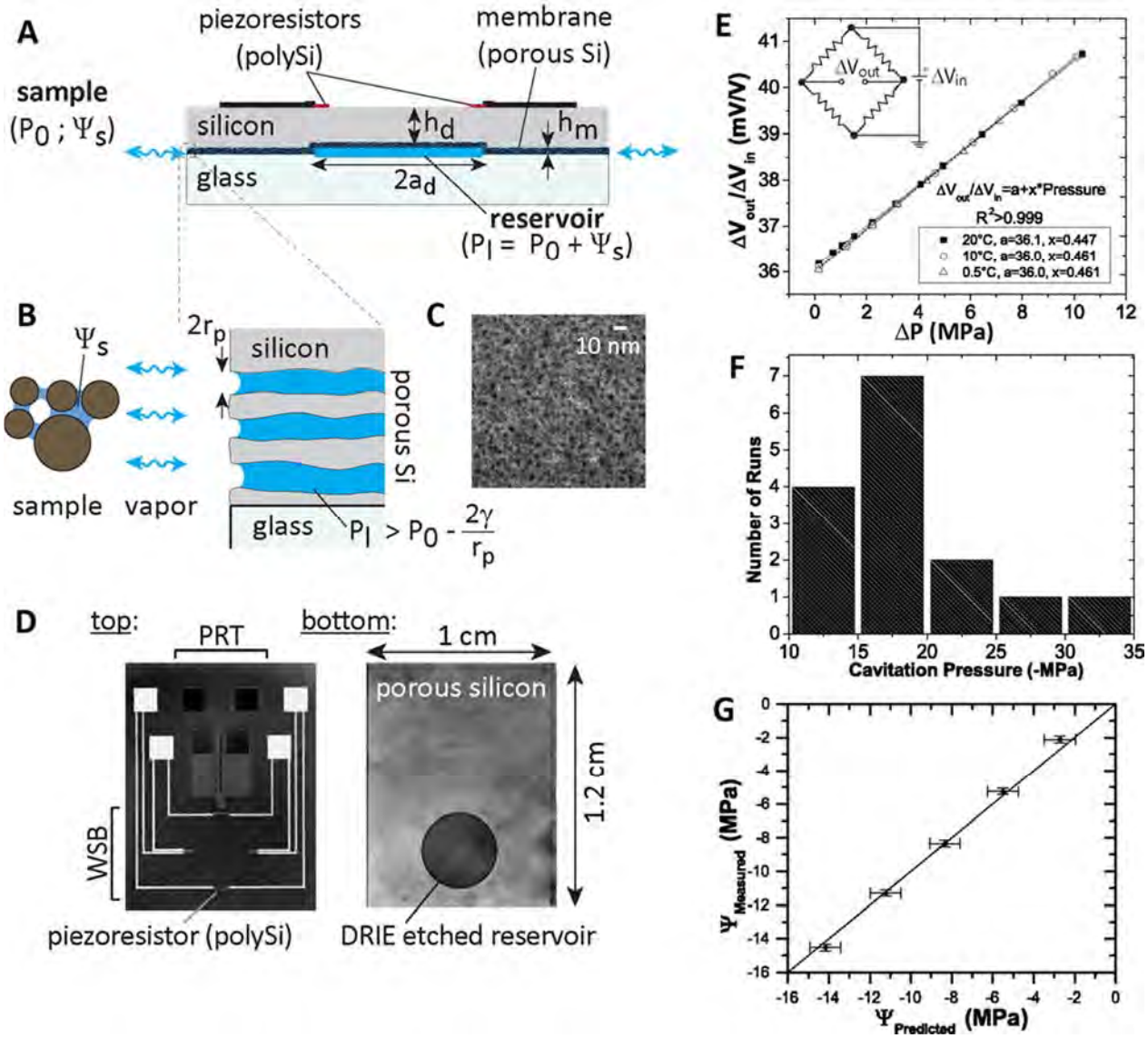

Figure 5: Mechanical measurements of negative pressures with a MEMS tensiometer. (**A**) Schematic cross-section of microtensiometer. The pressure in the liquid in reservoir drops into tension as it equilibrates with dry external environment through nano-porous membrane. (**B**) Schematic representation of local equilibrium at edge of porous silicon membrane. (**C**) Electron micrograph of porous silicon. (**D**) Optical micrographs of tensiometer. (**E**) Calibration of strain gauge (Wheatstone bridge of piezo resistors) at multiple temperatures and out to 10 MPa (100 bars). (**F**) Histograms of pressure (in negative MPa) at which cavitation was observed across 15 runs with ten devices as in (D). (**G**) Comparison of measured stress as a function of predicted stress to beyond -14 MPa.

the type shown in the micrograph in Fig. 2B. This structure allows us to minimize the thickness through which liquid must travel through the nano-porous structure (Fig. 3A). By coupling this membrane to 100s of micro-cavities formed in glass (fig. 3B) and allowing for equilibrium with decreasing relative humidity, we assessed the stability limit provided by this membrane. Fig. 3C presents the fraction of cavities that remained filled (uncavitated) as a function of relative humidity (bottom axis) and equivalent liquid pressure (top axis). We see that the membrane maintains 100% stability to pressures below -15 MPa (-150 bars), with some cavities remaining stable to nearly -30 MPa. ***This experiment demonstrates that structured membranes of the type required for our prototype SHLHP (Fig. 2) can be provide appropriately large tensions.***

Using a related format shown in **Figure 4A**, we have achieved even larger tensions and verified them by two methods. In this experiment, we again used a through etched porous silicon membrane, but the pores were of smaller dimension than in Fig. 3 (~1 nm radius rather than ~2-3 nm) and we sealed a free-standing wafer of porous silicon directly to glass without etched microchannels. We then measured the stability limit in these samples along two thermodynamic trajectories into negative pressure (Figs. 4B-C): the first is our standard, plant-mimetic technique in which we follow an isothermal path by allowing the liquid to come to metastable equilibrium with a sub-saturated vapor (Fig. 4B); the second, known as the Berthelot technique, starts with vapor-liquid coexistence in the cavity, warms the systems along the coexistence line until the liquid fills the cavity, and then cools the system along the liquid's isochore into tension (Fig. 4C). Fig. 4D reports the stability limits observed across multiple cavities and runs with a single sample along the isothermal path (purple squares) and the isochoric path (black diamonds). Along both paths, we observe pressures down to -60 MPa and, in the isothermal case to below -70 MPa. ***This experiment is significant for several reasons: 1) these tensions are the largest ever achieved in bulk liquids based on capillarity, 2) -70 MPa is the largest tension ever observed along an isothermal path, and 3) it is the first test of the stability limit along two distinct paths in a single sample and thus closes the door on the hypothesis that the stability limit shows path dependence[7].***

Axial transport and integration of sensing. In this funding period, we have successfully demonstrated two other components required for our vision of a SHLHP: 1) a mechanism for providing axial transport between micro-vessels and nanoporous membranes as is required for xylem-like transport in the liquid path (Fig. 2C), and 2) integration with direct sensing of pressure to provide diagnostic and control capabilities within the SHLHP (Fig. 2D). **Figure 5** presents an integrated technology formed with these elements, a MEMS tensiometer. As illustrated in Figs. 5A-C, this structure couples a microfluidic cavity filled with liquid to an external vapor via a layer of porosified silicon; a MEMS pressure sensor fabrication on the outside surface of the cavity measures the pressure in the internal volume of liquid. This device provides an exceptionally sensitive means of measuring departure from the saturated state in the environment. Following the convention of the plant science community, we represent this departure with the water potential: $\Psi \equiv [\mu - \mu_0(T)]/v_l$ [Pa], where μ [J/mole] is the chemical potential of water, $\mu_0(T)$ is the value at saturation, and v_l [m^3/mole] is the molar volume of the liquid phase. For a pure liquid, the water potential represents the deviation of pressure in the liquid from atmospheric: $\Psi_l = P_l - P_0$. For a vapor, that water potential depends on the vapor pressure as follows: $\Psi_v = (RT/v_l)\ln[p_v/p_{sat}(T)]$. By allowing the liquid and vapor to come to equilibrium ($\Psi_l = \Psi_v$), the tensiometer provides a direct measurement of the thermodynamic state of the external phase as a (negative) pressure.

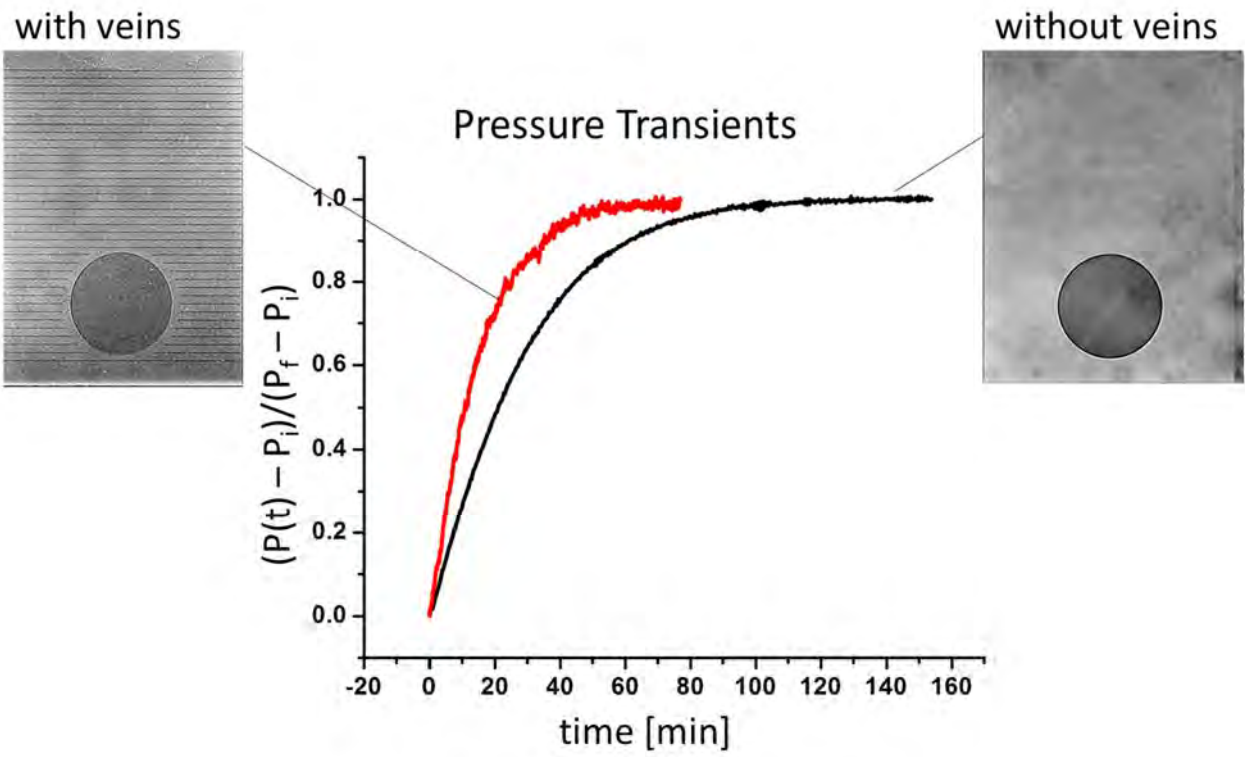

Figure 6: Management of tensiometer transients with artificial xylem. Normalized equilibration as a function of time in MEMS tensiometers as in Fig. 3. Equilibration occurs ~5 times faster when veins are included in the membrane structure (red curve – right-hand micrograph) than without veins (black curve – left-hand micrograph).

Fig. 5D presents top and bottom views of our MEMS tensiometer with a piezo-resistive strain gauge on the top and a reservoir within a layer of porous silicon on the bottom. Calibrations against known air pressures demonstrate clean, reproducible response (Fig. 5E)[5]. This system allows us to measure, for the first time, the negative pressures generated by metastable vapor-liquid equilibrium as a mechanical stress. Fig. 5F presents a histogram of the tension at which cavitation occurred over multiple tests in multiple devices. ***This direct measurement of the stability limit agrees with our previous, indirect evaluations, and confirms that we can reliably generate over 10 MPa (100 bars) of tension with porous silicon membrane. Furthermore, our measurement of pressures below -30 MPa represents the largest tension ever measured by mechanical means.*** In Fig. 5G, we compare measured values of water potential against those predicted with an extrapolated equation of state and find good agreement. This measurement provides a rare test of thermodynamic predictions in the superheated regime and demonstrates the accuracy of our instrument. ***The functionality of this device demonstrates the feasibility of building integrated technologies that operate deep in the superheated regime. This MEMS tensiometer also represents a valuable new analytical tool for plant and environmental science.*** We have one patent issued and a second pending on this system[8,9].

This platform has also provided us with a context in which to test the concept of artificial xylem presented in Fig. 2C: we can integrate microfluidic paths to provide high conductance over large distances with nanoporous membranes that allow for the generation of large tensions. The inset on the left in **Figure 6** shows a tensiometer with vessel segments partially spanning the

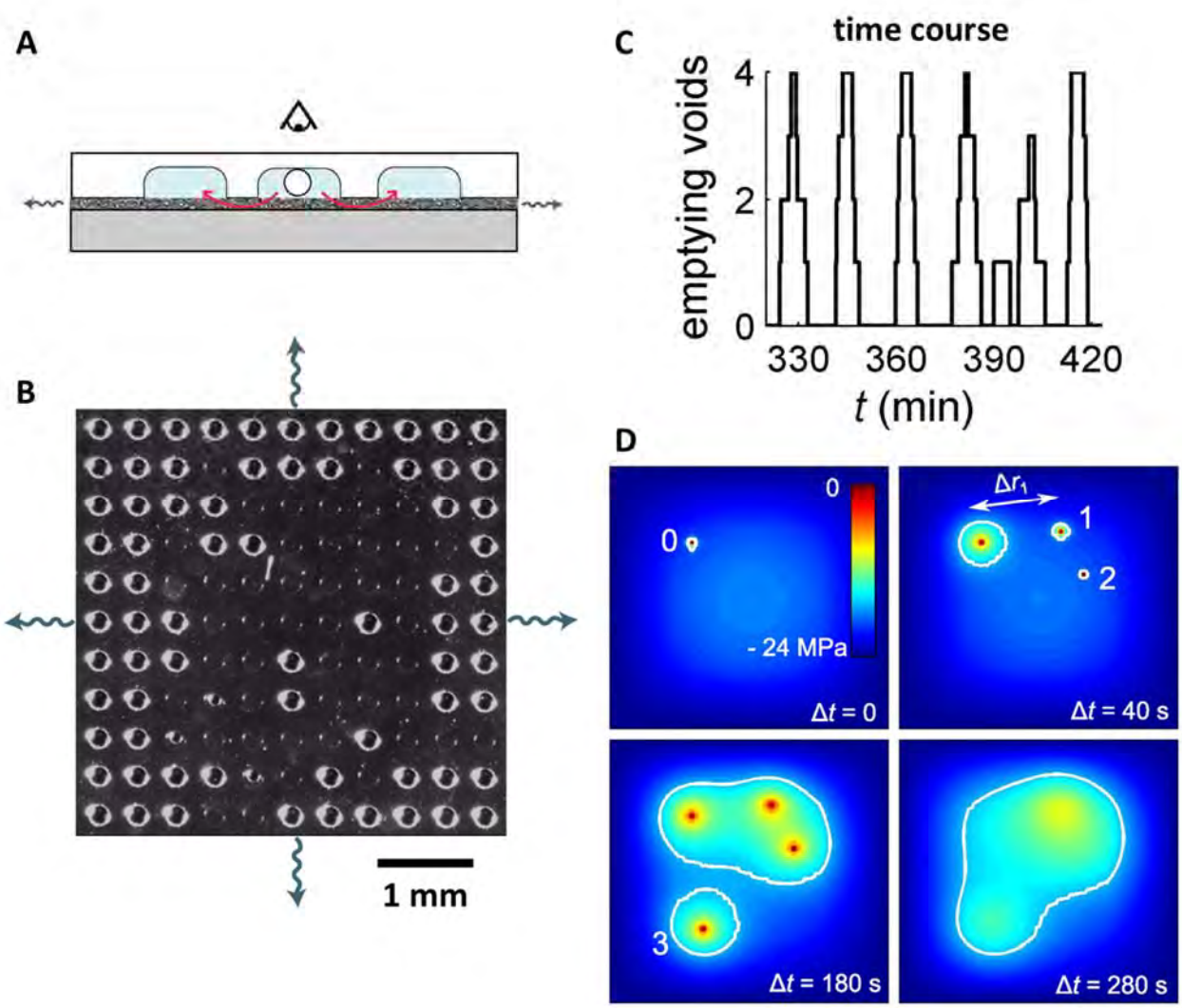

Figure 7: Dynamics of cavitation in synthetic xylem. (**A**) Schematic cross-sectional view of synthetic xylem structure with microfluidic cavities coupled to one another and to outside environment through nanoporous silicon. (**B**) Micrograph showing top-view of an internal region of synthetic xylem during drying. Empty cavities have a bright outline; full cavities are dark. Growing bubbles are visible in cavities that are actively emptying. (**C**) Time course of emptying events taken from a sample as in (B). Periodic events continue during entire duration of drying of cavities. (**D**) Predictions from simulation of drying and cavitation in a sample as in (B). One period of cavitation and emptying (corresponding to one peak in (C) is shown. Color map represents liquid pressure. Upon cavitation, the pressure in a cavity goes from a negative value (blue) to the saturation vapor pressure (red) and the adjacent regions of the sample are resaturated (green zones). White curve corresponds to typical cavitation pressure.

gap between the reservoir and the external edge of the porous silicon membrane. At each end of these vessels, the liquid passes through the porous silicon. This architecture mimics the structure of xylem with vessel segments interconnected by nanoporous membranes (border pit membranes)[10]. ***As illustrated by the significant reduction in the duraction of the transient in pressure (~ 5×) with the inclusion of these vessels, this design strategy provides an effective means of controlling the resistance of the liquid path.***

Objective 3: Elucidate plant physiological mechanisms of operation and repair for the manipulation of liquids at large negative pressures.

We have exploited the experimental and theoretical tools described above to investigate features of plant physiology that allow for robust function during transpiration at negative pressures.

Transport and phase change in micro-nanofluidic systems. As discussed above, a ubiquitous feature of the conductive tissues of plants is the interconnection of micro- and nano-scale passages along the liquid path. These structures provide efficient flow, large capillary pressures, and a redundancy that protects against catastrophic failure when cavitation occurs[10]. As illustrated in Fig. 6, we have the ability to capture such structure in microfluidic structures formed of glass and silicon. In this funding period, we have used this ability to study the characteristics of flow and cavitation in such composite structures. **Figures 7A-B** present a

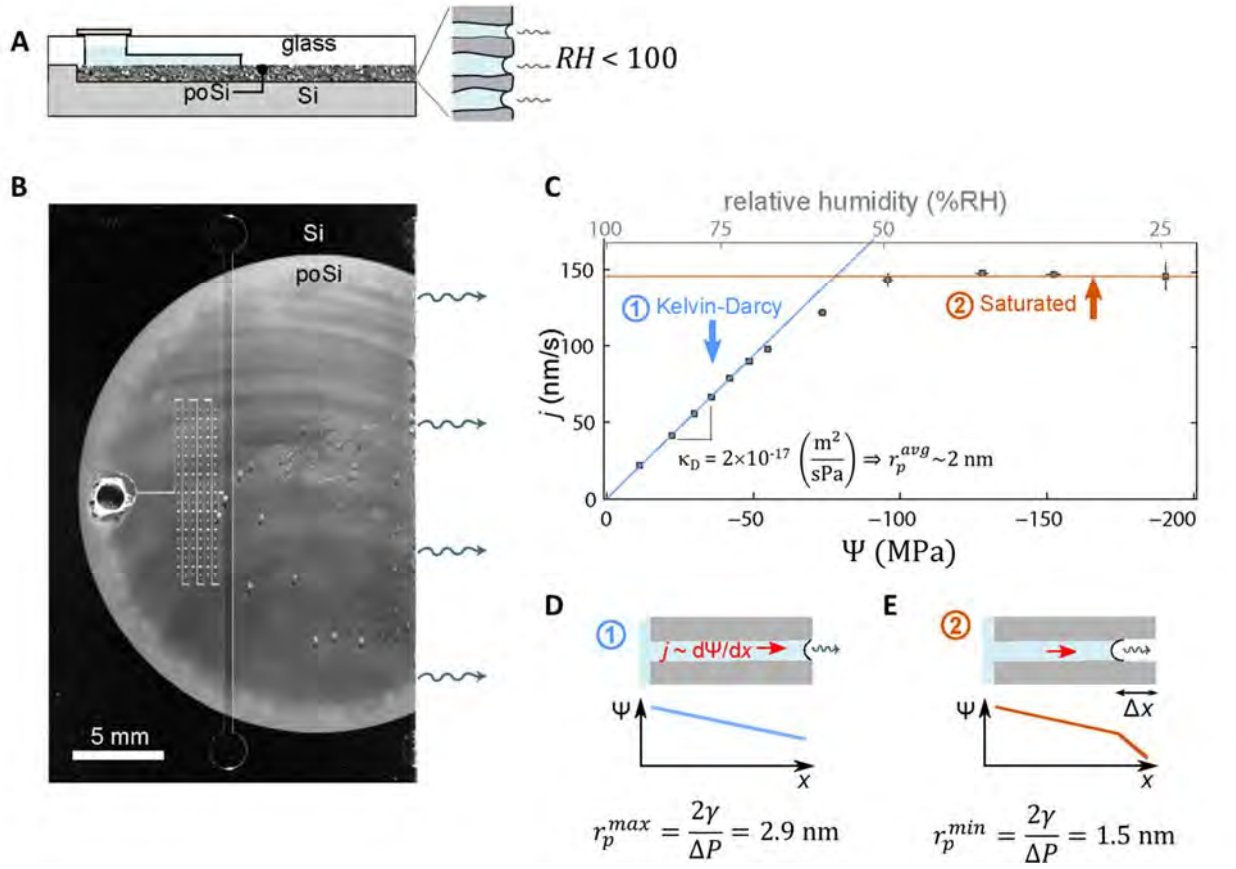

Figure 8: Quantitative measurements of transpiration driven flow in nano-porous membrane. **(A)** Schematic cross-sectional view of device that couples a microfluidic structure to a zone of nano-porous silicon. (**B**) Micrograph showing top-view of device. A serpentine microchannel allows flow to be measured with the displacement of a meniscus as water is drawn through porous silicon by transpiration in an atmosphere of controlled relative humidity, *RH*. (**C**) Steady state perfusion speed as a function of *RH* (top axis) and equivalent pressure at evaporative edge (bottom axis). The flow speed grows linearly with pressure out to ~ -50 MPa (Kelvin-Darcy regime) and then saturates to a constant value. Darcy permeability, κ_D and implied average pore radius, r_p^{avg} are reported. (**D-E**) Schematic representations of proposed scenarios corresponding to (1) Kelvin-Darcy regime and (2) Saturated regime. Implied maximum radius, r_p^{max} and minimum radius, r_p^{min} are reported.

simple geometry in which we performed these experiments: circular micro-cavities in glass are coupled to each other and the external environment via a layer of nanoporous silicon[6]. Upon exposure to a dry external environment, water evaporates from the composite material and brings the liquid in the cavities to negative pressures that can induce cavitation. The cavitation events across this array of cavities proceed in an extremely regular fashion, in periodic bursts (Fig. 7C); the regularity of these bursts persists through the drying process for 100s of cavities. Such intermittency suggests the presence of a strong, non-linear coupling within the dynamics. In investigating the origin of this effect, we considered both acoustic and hydraulic coupling. We established that hydraulic coupling in the form of poroelastic relaxation within the composite matrix could explain the behavior quantitatively. Fig. 7D illustrates this mechanism with a simulation of the dynamic pressure field during one burst of four cavitation events: upon cavitation (Δt = 0), the pressure in a cavity jumps from a negative value (blue) to the saturation vapor pressure (red) and a diffusive wave of pressure propagates out as liquid is released from the cavity; this propagation is tracked by the white isobar. Before the relaxation has propagated across the entire sample, additional cavitation events can occur (Δt = 40 s). Once the relaxation has spread across the sample, metastability is relieved and further cavitation is suppressed (Δt = 180 and 240 s). ***Further evaporation then reestablishes tension within the sample and the cycle repeats. This theory provides a quantitative explanation of the observed response and a***

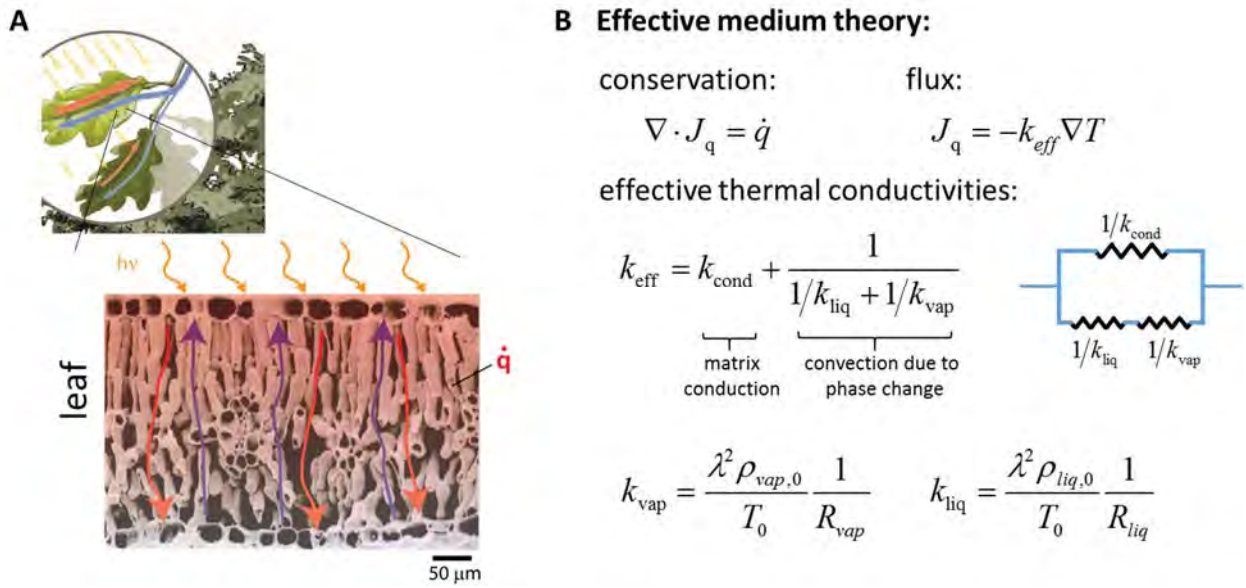

Figure 9: Effective medium theory of heat transfer in a cellular composite. **(A)** Electron micrograph of leaf cross-section. Indicated schematically are incident light, thermal adsorption in the bulk ($\dot{q}$ [W m^{-3}]), and convective flows of liquid (blue arrows) and vapor (red arrows). Evaporation drives vapor flows from hot to cold regions; wicking drives liquid in the matrix from cold to hot regions. **(B)** Effective medium expressions for steady state heat transfer within an isotropic cellular composite with heat generation in the bulk. The effective thermal conductivity, k_{eff} [W m^{-1} °C^{-1}] takes the form of a conductive resistance ($1/k_{cond}$) in parallel with resistances associated with the convection of the liquid ($1/k_{liq}$) and vapor ($1/k_{vap}$). The effective conductivities associated with convection can be expressed in terms of properties of the working fluid (latent heat, λ [J kg^{-1}] and densities, $\rho_{liq,0}$ and $\rho_{vap,0}$ [kg m^{-3}]) at the characteristic temperature T_0 and the resistances flow of the liquid and vapor through the structure (R_{liq} and R_{vap} [s^{-1}])

new basis for understanding the dynamics observed during draught stress in plants and in the processing of advanced materials such as porous dielectrics[6].

We have exploited a related system (**Figure 8**) to interrogate the characteristics of liquid transport in the extreme confinement (2-4 nm-diameter pores) imposed by the nanoporous silicon membrane. Significant debate persists regarding the validity of continuum transport theories and bulk thermodynamics in this limit[11]. In this system, we drain a serpentine microfluidic channel via transpiration through a layer of porous silicon (Figs. 8A-B); by tracking the meniscus within this channel, we can follow minute flows with high precision. Fig. 8C reports observed rate of the permeation flow as a function of the water potential, Ψ in the external vapor. These data illustrate several important points: 1) for driving forces to beyond -50 MPa, the flow grows linearly with Ψ; this response indicates that the thermodynamic relations the define Ψ remain valid even with the liquid confined within nanoscopic pores and that the capillary pressures generated by these pores can reach upward of 500 bars. 2) The implied permeability in this regime implies a typical pore radius of ~2 nm, in close agreement with conventional measurements by conventional porimetry[6]. This agreement indicates that continuum laws of fluid mechanics hold despite the confinement. 3) For larger stresses, the flow speed saturates to a constant value that persists to beyond -150 MPa (-1,500 bars). This saturation provides a basis for creating a robust current source, i.e., with constant flow over a wide range of environmental conditions. 4) Simple hypotheses explain the observed regimes – linear response (Fig. 8D) and saturation (Fig. 8E) – and provide additional measures of the nanostructure of the porous silicon membrane that are again consistent with conventional porimetry. ***With these and additional experiments (not shown), we have provided an unusually coherent picture of the thermodynamics, transport, and capillarity with strong confinement. These results provide an important grounding for the design of nanofluidic technologies and the interpretation of biological transport processes as in the xylem of plants.***

Coupled heat and mass transfer in plant tissues.

In a collaboration led by Dr. Fulton Rockwell, a shared post-doc between Harvard and Cornell, we have developed a set of transport theories for the unsaturated porous tissues within the leaves of plants[12-14]. These theories inform our understanding of how leaves manage the solar thermal load and how the resistance to transpiration flux is distributed between liquid and vapor paths within the leaf (**Figure 9A**). We built our theory of coupled heat and mass transfer with the machinery of non-equilibrium thermodynamics[12]. This approach provides simple,

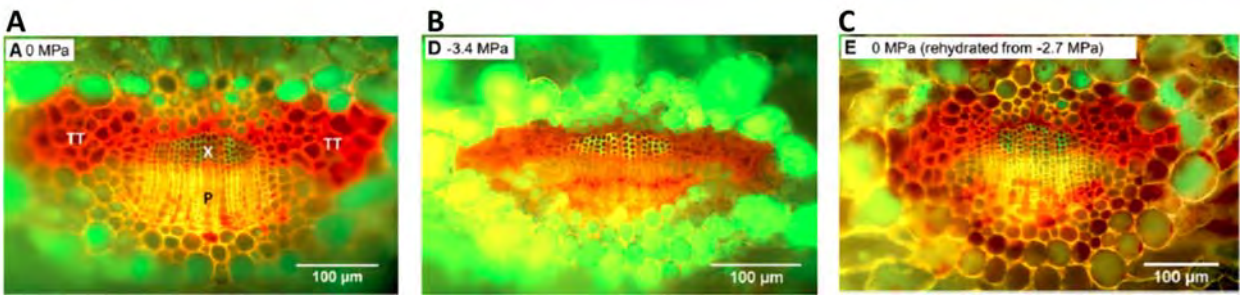

Figure 10: Autonomic response of xylem conductance in conifer needle. (**A-C**) Confocal fluorescence micrographs of cross-sections of needles. In red are xylem vessels. These vessels are open at 0 MPa of stress (A), collapsed at -3.4 MPa of stress (B) and reopened upon rehydration to 0 MPa of stress.

compact expressions for the fluxes in terms of experimentally measurable parameters and we were able to apply it successfully to a series of experiments on leaves from various species. Interestingly, we were also able to map the theory onto the expressions for effective thermal conductances that we had developed independently in our model of LHPs (Figure 9B)[2]. With this realization, we have been able to build a general effective medium theory for unsaturated porous materials: as illustrated in Fig. 9B, each element of the material can be represented by an equivalent thermal circuit in which phase change processes (k_{liq} and k_{vap}) operate in parallel with the background conduction through the solid matrix (k_{cond}). The theory provides simple expressions for k_{liq} and k_{vap} in terms of the properties of the working fluid (latent heat, λ and density, ρ) and the hydraulic resistance of the matrix for liquid (R_{liq}) and vapor (R_{vap}) flow. ***This theory forms an excellent basis for the design of synthetic composites with tunable heat transfer properties. We are pursuing this opportunity in the current funding period.***

Autonomic regulation of permeability within xylem tissue. During this funding period, we have critically examined a number of the experiments that have informed the plant physiology community's thinking about the response of xylem tissue to draught stress[15-17]. Importantly, we have elucidated a major source of potential artifacts in the methods used to measure the loss of conductance in the xylem[15,16]. In particular, we have shown that in many circumstances, air bubbles may be introduced into the xylem during sample preparation, and we have presented alternative techniques that minimize this artifact. As an important outcome from this development, we suggest that many species may not allow for significant cavitation accept under the most severe drought conditions and, furthermore, recovery of conductance upon reduction of stress may have been misinterpreted as refilling of embolized vessels[16]. In parallel, we have shown that a distinct mechanism underlie the modulation of conductance by drought stress in some species[17]. As shown in **Figure 10**, we observe significant deformation in the conductive tissue in conifer needles as stress approaches those at which loss of conductance is

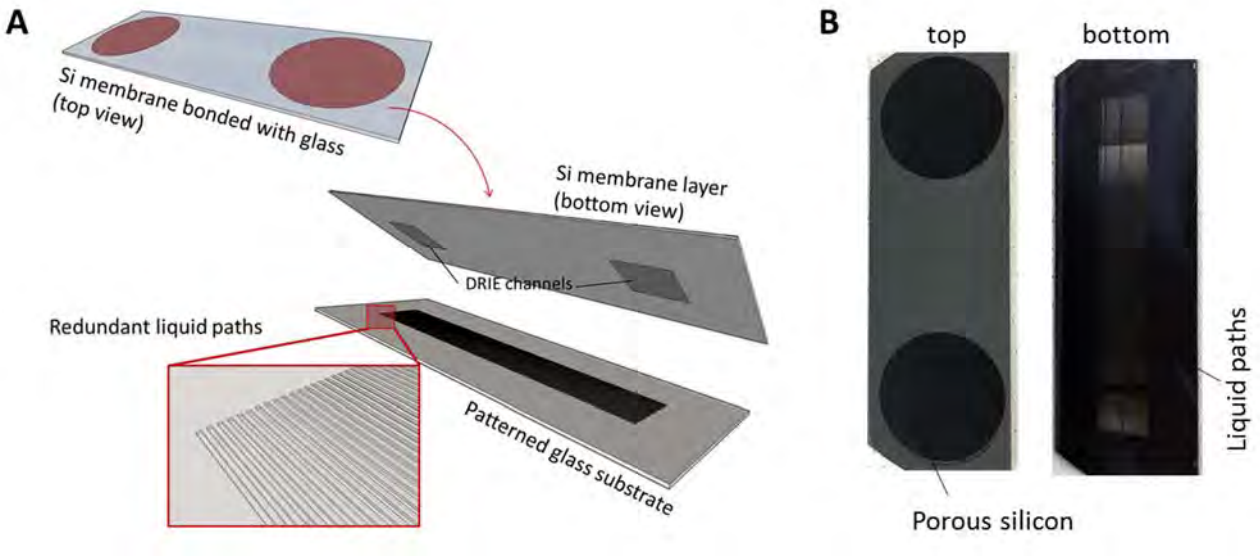

Figure 11: Wick structure for superheated loop heat pipe. (**A**) Schematic representation of wick formed of anodically bonded silicon and glass. (**B**) Photographs showing top and bottom views of wick.

observed (left frame at 0 stress to middle frame at -3.4 MPa). Furthermore, this deformation relaxes upon relief of the stress (right frame), corresponding to the recovery of the unstressed conductance. We suggest that certain species tune the mechanics of the xylem tissue to enable this reversible change in conductance due to collapse of the vessels. ***This alternative mechanism of regulation has important implications for our understanding of drought response and provides new design concepts for technologies that operate with liquids under tension.***

Objective 4: Development and characterization of prototype SHLHP:

As illustrated in Figs. 2-8, we have made important progress in the development of the components necessary for a SHLHP and in our understanding of their design and operation. Over the past year, we have worked toward uniting these components into a first full prototype of a SHLHP. In particular we have brought together the hierarchically structured membrane (Figs. 2B and 3) and a version of redundant microchannels (Fig. 2C). **Figure 11** presents our complete liquid path (wick) (Fig. 11A): in a silicon wafer, we define symmetrical evaporator and condenser zones by forming a 50 μm-thick layer of porous silicon by anodic etching and microchannel vias by deep reactive ion etching (DRIE); in a glass wafer, we define a redundant set of microchannels that span the distance between the evaporator and the condenser; and, finally, we align and bond the glass and silicon to close the system. Fig. 11B presents photographs of the completed wick structure. Unfortunately, the current set of wick structures shows unexpectedly low stability relative to what we found with preliminary tests as in Fig. 3:

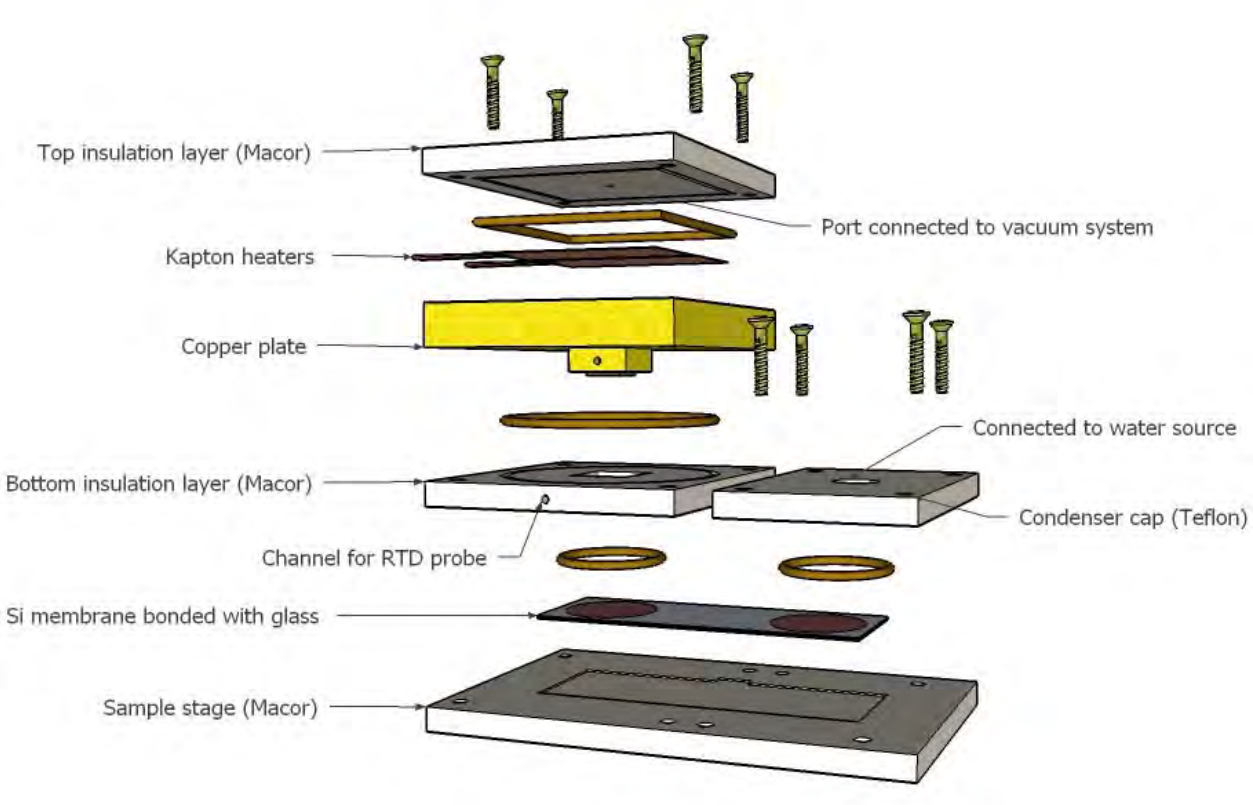

Figure 12: Schematic representation of test system for SHLHP prototype.

we observe significant cavitation of the vessels for tensions as low as 3 MPa and complete loss of connectivity by 6 MPa (compare to 100% stability out to -15 MPa in Fig. 3). We are currently diagnosing this problem and attempting various strategies to rectify it. Our current hypotheses are that there exist rare defects in the porous silicon that allow vapor entry into the vessels. To test this hypothesis and attempt to repair the structures, we are depositing poly(electrolyte) multilayers onto the membranes, a method that have been shown to shrink the distribution of pore sizes in other membrane applications, as reviewed by Joseph et al.[18]. Our alternative hypothesis is that the silicon wafers were not sufficiently well polished and left nanochannels at the silicon-glass interface along which air can enter the vessels. This defect may not be repairable and pushes us toward more careful sourcing and characterization of our wafers. Finally, we point out that our design of our liquid paths in this first prototype does not take advantage of segmentation with nanoporous membranes separating adjacent vessels, as in xylem and in our artificial xylem (Figs. 2C, 6 and 7). In future iterations, we will employ this added protection against the spread of vapor pockets within the liquid path.

In anticipation of soon having successful wick structures capable of moving liquids at large negative pressures, we have designed and built an experimental system that will allow us to fully characterize the operation of our SHLHP design and compare it against conventional designs and modes of operation. **Figure 12** presents this system. Importantly, this design allows for fine control of the vapor pressure experienced at the evaporator surface. This control allows us to simulate a continuum of modes of operation between the pure superheated mode and the conventional mode. Further, at the condenser end we have the option to run with and without a membrane and thus create either the saturated or unsaturated mode of operation. These experiments will provide a complete test of the design concepts and predictions that we have presented to date[2].

V. Future directions.

Model and design: We will focus our future modeling effort in several areas: 1) a local model of the heat transfer and evaporation process in the evaporator at the scale of the individual solid contacts and vapor channels. This model will help us optimize the design of the evaporator zone to fully exploit the available evaporative surface. 2) An application of the effective medium theory in Fig. 9 to specific geometries with a focus on the design of thermal metamaterials that exploit the exceptional conductivity and low capacitance provided by phase change processes.

Components and integration: As discussed above, our first priority is the successful realization of a wick for the SHLHP following the design outlined in Fig. 11. Are current and future effort focuses on eliminating defects that lower the stability limit and on new designs of the liquid paths that localize failure and provide redundancy. In parallel, we are exploring the use of alternative materials to serve as nanoporous membranes. In particular, we believe that nanoporous glasses provide an attractive alternative for some applications and would provide a route to scaling out the SHLHP designs to larger dimensions.

Biology: In the coming period, we are working to apply our detailed model of transport processes in the leaf within a system biology framework that aims to identify the key mechanism by which the plant senses and responds to drought stress via active biological processes. We are also completing a set of models of phloem function that are providing valuable insights into the various mode by which plants export photosynthetic products. These models have also provided the basis for forming microfluidic pumping systems in collaboration with a team at MIT.

V. Bibliography

1. Stroock, A. D. & Wheeler, T. High Performance Wick. USA patent 12/990,845 (2009).
2. Chen, I. T. *et al.* Analysis of Superheated Loop Heat Pipes Exploiting Nanoporous Wick Membranes. *Aiche J.* 60, 762-777 (2014).
3. Faghri, A. *Heat Pipe Science and Technology*. (Taylor and Francis, 1995).
4. Wheeler, T. D. & Stroock, A. D. The transpiration of water at negative pressures in a synthetic tree. *Nature* 455, 208-212 (2008).
5. Pagay, V. *et al.* A microtensiometer capable of measuring water potentials below -10 MPa. *Lab on a Chip* 14, 2806-2817 (2014).
6. Vincent, O. *et al.* Drying by Cavitation and Poroelastic Relaxations in Porous Media with Macroscopic Pores Connected by Nanoscale Throats. *Physical Review Letters* 113 (2014).
7. Caupin, F. & Stroock, A. D. in *Liquid Polymorphism* Vol. 152 *Advances in Chemical Physics* (ed H. E. Stanley) 51-80 (John Wiley & Sons Inc, 2013).
8. Stroock, A. D. *et al.* Microtensiometer sensor, probe and method of use. 13/264,964 8,695,407 (2014).
9. Stroock, A. D. *et al.* Microtensiometer sensor, probe and method of use. 61/835,224 (submitted on June 14, 2013).
10. Stroock, A. D. *et al.* The Physicochemical Hydrodynamics of Vascular Plants. *Annu. Rev. Fluid Mech.* 46, 615-642 (2014).
11. Bocquet, L. & Tabeling, P. Physics and technological aspects of nanofluidics. *Lab on a Chip* 14, 3143-3158 (2014).
12. Rockwell, F. E. *et al.* The Competition between Liquid and Vapor Transport in Transpiring Leaves. *Plant Physiol.* 164, 1741-1758 (2014).
13. Rockwell, F. E. *et al.* Leaf hydraulics I: Scaling transport properties from single cells to tissues. *J. Theor. Biol.* 340, 251-266 (2014).
14. Rockwell, F. E. *et al.* Leaf hydraulics II: Vascularized tissues. *J. Theor. Biol.* 340, 267-284 (2014).
15. Wheeler, J. K. *et al.* Cutting xylem under tension or supersaturated with gas can generate PLC and the appearance of rapid recovery from embolism. *Plant Cell Environ.* 36, 1938-1949 (2013).
16. Rockwell, F. E. *et al.* Cavitation and Its Discontents: Opportunities for Resolving Current Controversies. *Plant Physiol.* 164, 1649-1660 (2014).
17. Zhang, Y. J. *et al.* Reversible Deformation of Transfusion Tracheids in Taxus baccata Is Associated with a Reversible Decrease in Leaf Hydraulic Conductance. *Plant Physiol.* 165, 1557-1565 (2014).
18. Joseph, N. *et al.* Layer-by-layer preparation of polyelectrolyte multilayer membranes for separation. *Polymer Chemistry* 5, 1815-1831 (2014).

1.

1. Report Type

F na Report

Primary Contact E-mail

Contact email if there is a problem with the report.

ads10@corne .edu

Primary Contact Phone Number

Contact phone number if there is a problem with the report

607-255-4276

Organization / Institution name

Corne Un vers ty

Grant/Contract Title

The full title of the funded effort.

PLANT-MIMETIC HEAT PIPES FOR OPERATION WITH LARGE INERTIAL AND GRAVITATIONAL STRESSES

Grant/Contract Number

AFOSR assigned control number. It must begin with "FA9550" or "F49620" or "FA2386".

FA9550-12-1-0227

Principal Investigator Name

The full name of the principal investigator on the grant or contract.

Abraham Stroock

Program Manager

The AFOSR Program Manager currently assigned to the award

Byung L p Lee

Reporting Period Start Date

05/01/2012

Reporting Period End Date

04/30/2015

Abstract

The des gn of heat transfer systems for app cat ons n a rcraft and other dynam c contexts nvo ves str ngent constra nts on we ght, form factor, breadth of operat ng cond t ons, and robustness of operat on. Heat p pes have ong been recogn zed as an attract ve, pass ve a ternat ve to convent ona heat exchangers for these app cat ons. Yet, the cap ary m tat on n convent ona heat p pes m ts the r operat on to contexts n wh ch there ex st m n ma hydrau c, grav tat on, and nert a stresses. In th s project, we have exp o ted ns ghts from the phys o ogy of p ants to propose p ant- nsp red des gns of oop heat p pes for operat on w th arge stresses. Toward the rea zat on of these Superheated Loop Heat P pes (SHLHP), we deve oped a set of mathemat ca mode s and exper menta approaches. Our mode s prov de des gn ru es for heat transfer systems that cou d prov de s gn f cant advantages re at ve to convent ona des gns. Our exper menta p atforms have ed to unprecedented measurements on qu ds at arge negat ve pressures, ns ghts nto the dynam cs of metastab e qu ds, and the prototypes of the f rst techno og es to exp o t qu ds under tens on. Our work has a so prov ded new ns ghts about p ant mechan sm of transport that w nform our future efforts on th s project.

Distribution Statement

This is block 12 on the SF298 form.

D str but on A - Approved for Pub c Re ease

Explanation for Distribution Statement

If this is not approved for public release, please provide a short explanation. E.g., contains proprietary information.

SF298 Form

Please attach your SF298 form. A blank SF298 can be found here. Please do not password protect or secure the PDF The maximum file size for an SF298 is 50MB.

Stroock_AFD-070820-035.pdf

Upload the Report Document. File must be a PDF. Please do not password protect or secure the PDF . The maximum file size for the Report Document is 50MB.

AFOSR_FA9550-12-1-0227_Stroock_f na _report_06_2015_FIGURES.pdf

Upload a Report Document, if any. The maximum file size for the Report Document is 50MB.

Archival Publications (published) during reporting period:

1. Sant ago, M., Pagay, V. V. & Stroock, A. D. Impact of E ectrov scos ty on the Hydrau c Conductance of the Bordered P t Membrane: a Theoret ca Invest gat on. P ant Phys o ogy, 163, 999-1011 (2013).
2. Rockwe , F. E. , Ho brook, N. M. & Stroock, A. D. Leaf hydrau cs I: Sca ng transport propert es from s ng e ce s to t ssues. Journa of Theoret ca B o ogy, 340, 251–266 (2014).
3. Rockwe , F. E. , Ho brook, M. N. & Stroock, A. D. Leaf hydrau cs II: Vascu ar zed t ssues. Journa of Theoret ca B o ogy, 340. 267–284 (2014).
4. Rockwe , F. E. , Ho brook, N. M. & Stroock, A. D. The compet t on between qu d and vapor transport n transp r ng eaves. P ant Phys o ogy 164, 1741-1758 (2014).
5. Chen, I.-T., Pharkya, A. & Stroock, A.D. Ana ys s of Superheated Loop Heat P pes Exp o t ng Nanoporous W ck Membranes. AIChE Journa , 60, 762-777 (2014).
6. Stroock, A. D., Pagay, V.V., Zw en eck , M. A. & Ho brook, N. M. The phys cochem ca hydrodynam cs of vascu ar p ants. Annua Rev ew of F u d Mechan cs, 46, 615-642 (2014).
7. Pagay, V., Sant ago, M., Sessoms, D.A., Huber, E.J., V ncent, O., Pharkya, A.§ Corso, T.N., Lakso, A.N. & Stroock, A.D. A m crotens ometer capab e of measur ng water potent a s be ow -10 MPa. Lab-on-a-ch p, 14, 2806-2817 (2014).
8. V ncent, O. , Sessoms, D.A., Huber, E.J., Gu oth, J. & Stroock, A.D. Dry ng by cav tat on and poroe ast c re axat ons n extreme nk-bott e porous med a. Phys ca Rev ew Letters, 113, 134501 (2014).
9. Zhang, Y.-J., F.E. Rockwe , J.K. Whee er and N.M. Ho brook. Revers b e deformat on of transfus on trache ds n Taxus baccata s assoc ated w th a revers b e decrease n eaf hydrau c conductance. P ant Phys o ogy 165, 1557-1565 (2014).
10. Rockwe , F.E., J.K. Whee er and N.M. Ho brook. Cav tat on and ts d scontents: opportun t es for reso v ng current controvers es. P ant Phys o ogy 164, 1649-1660 (2014).
11. Whee er, J. K., Huggett, B. A., Tofte, A. N., Rockwe , F. E. & Ho brook, N. M. Cutt ng xy em under tens on or supersaturated w th gas can generate PLC and the appearance of rap d recovery from embo sm. P ant Ce Env ron. 36, 1938-1949 (2013).
12. Carro , N. J., Jensen, K. H., Parsa, S., Ho brook, N. M. & We tz, D. A. Measurement of F ow Ve oc ty and Inference of L qu d V scos ty n a M crof u d c Channe by F uorescence Photob each ng. Langmu r 30, 4868-4874 (2014).

PATENTS

1. Stroock, A.D., Lakso, A.L., Pagay, V., L c, B. & Metz er, M. M crotens ometer sensor, probe and method of use. USA Patent No. 8,695,407 (ssued 2014).
2. Stroock, A.D., Lakso, A.L., Pagay, V., Sant ago, M., Sessoms, D. Mu t moda sensor, method of use, and method of fabr cat on. App cat on No. PCT/US14/42435 (app ed 2014).

Changes in research objectives (if any):

N/A

Change in AFOSR Program Manager, if any:

N/A

Extensions granted or milestones slipped, if any:

N/A

AFOSR LRIR Number

LRIR Title

Reporting Period

Laboratory Task Manager

Program Officer

Research Objectives

Technical Summary

Funding Summary by Cost Category (by FY, $K)

	Start ng FY	FY+1	FY+2
Sa ary			
Equ pment/Fac t es			
Supp es			
Tota			

Report Document

Report Document - Text Analysis

Report Document - Text Analysis

Appendix Documents

2. Thank You

E-mail user

Jun 30, 2015 08:39:31 Success: Ema Sent to: ads10@corne .edu